J. Fluid Mech. (1978), *vol.* 85, *part* 1, *pp.* 161–186
Printed in Great Britain

The behaviour of naturally oscillating three-dimensional flow around a cylinder

By CLAUDE TOURNIER
Institut Universitaire de Technologie, Valenciennes, France

AND BERNARD PY
Institut Universitaire de Technologie, Brest, France

(Received 15 November 1975 and in revised form 17 January 1977)

Split-film electrochemical transducer theory is briefly outlined so as to show its ability to separate statistical properties of each component of the surface velocity gradient in regions as different as a boundary layer, a separated zone and a three-dimensional separation line. A lot of measurements of the flow field near a cylinder which are not yet available elsewhere are carried out everywhere on the cross-section of a yawed cylinder. A direct verification of the independence principle and Wild's thermal analogy in separated zones is executed. The periodic and random parts of each component of the surface velocity gradient are separated. Cross-spectral analysis between any pair of points shows that the periodic surface flow is coherent upon any cross-section and in a large region in the spanwise direction. The stationary wave system is investigated in space and time. The reconstitution, instant by instant, of the averaged integral wall streamlines leads to an understanding of the synchronization of the natural oscillations. The four main stagnation or separation lines quickly move from one extreme position to the other, and at certain times contrary vortices stretching in the direction of the generators can appear. In the rearward stagnation region random small-scale fluctuations are probably turbulent, but in the intermediate region high-level random fluctuations in the spanwise direction are much more coherent and probably contribute to keeping the flow in phase at large distances.

1. Introduction

Experimental investigation of wall streamline patterns (or integral lines of the wall shear stress direction field) is a powerful method for analysing the validity of mathematical processing which is applied to three-dimensional flows. Visualization techniques are generally used (for example, Werlé 1959, 1960, 1962). However, for unsteady flows, the streamlines are distinct from the particle trajectories. Otherwise, when the flow becomes turbulent, random small-scale movements and the diffusion effect which results make elucidation from snapshots more complex. The aim of an instrumental technique is to provide directly velocity values which are not dependent on the previous history of fluid particles. Also, appropriate data processing could allow reconstitution of the instantaneous flow pattern without taking into account the local perturbations introduced by turbulence.

Such an investigation in three-dimensional unsteady flows, which is one of the purposes of the present work, does not seem to have been available up to now. However, many successive improvements illustrate the usefulness of electrochemical techniques in the measurement of the components of the surface velocity gradient in three-dimensional flows. With a large aspect ratio electrode, Mitchell & Hanratty (1966) achieved a transducer sensitive to the flow direction. Karabelas & Hanratty (1968) used a cross-array which allows flow directions in one quadrant to be measured. Two sandwiched electrodes avoid ambiguities and measurements in all four quadrants are feasible. The chevron array of Sirkar & Hanratty (1970) is both more simple and more sensitive but is not suitable when the flow direction deviates from the sector bounded by the two electrodes. Directional properties of split-film electrochemical transducers have been calculated or measured by Py (1973) for various configurations and aspect ratios. Some of these are constructed from two joined but insulated platinum ribbons which are cut flush with the surface. For this case, figure 1 (plate 1) shows the appearance of the two conducting areas. These split transducers are easy to shape and their spatial resolution is good. The flow direction can be determined in two quadrants only, but as no ambiguities exist for one component of the velocity gradient, split electrodes are suitable in investigations of separated flow. Intensive use of these last transducers is made in this work so as to measure the main characteristics of the naturally oscillating flow around the cross-section of a circular cylinder. They allow measurement of not only the local statistical properties of the flow, but also the joint statistical properties between one point and any other.

As unsteady pressure measurements are feasible whatever the azimuth is, it appears that the characteristics which are the best known are those of the instantaneous static pressure field (see, for example, Loiseau & Szechenyi 1972; Surry 1972; Batham 1973). But as far as the velocity field is concerned, the results are fragmentary and few significant measurements are available close to the wall in separated zones. Bellhouse & Schultz (1966) used a hot film and examined the limit of validity of boundary-layer theory. McCroskey & Durbin (1972) also developed thermal techniques, using the pair of hot films with which Dwyer & McCroskey (1973) detected backflows. In general the transfer coefficient of thermal transducers is important in regions of low velocity, which somewhat complicates the data processing. Direct measurements of the surface velocity gradient have been made by Dimopoulos & Hanratty (1968) and Son & Hanratty (1969). The latter authors gave in detail the qualitative aspects of the natural fluctuations in the flow. In particular they showed by visualization techniques that spanwise velocity fluctuations can predominate downstream of the separation line. This result, however, restricts the validity of the indications available in these regions from a single-electrode transducer. Using a directionally sensitive probe registering static pressure differences, Achenbach (1968) made measurements in regions of backflow, but very large fluctuations certainly caused errors owing to the nonlinearity of the transducer. Unsteady characteristics of the flow cannot be measured by this method.

This paper outlines as briefly as possible the theory of split electrochemical transducers so as to show how the direction and the value of surface velocity gradients can be obtained. Experiments conducted all round the cross-section of a circular cylinder for a Reynolds number of 13900 are then described. The yawing was systematically executed to meet three conditions: (i) to generate at every point a spanwise time-averaged velocity component more important than the fluctuations; (ii) to avoid

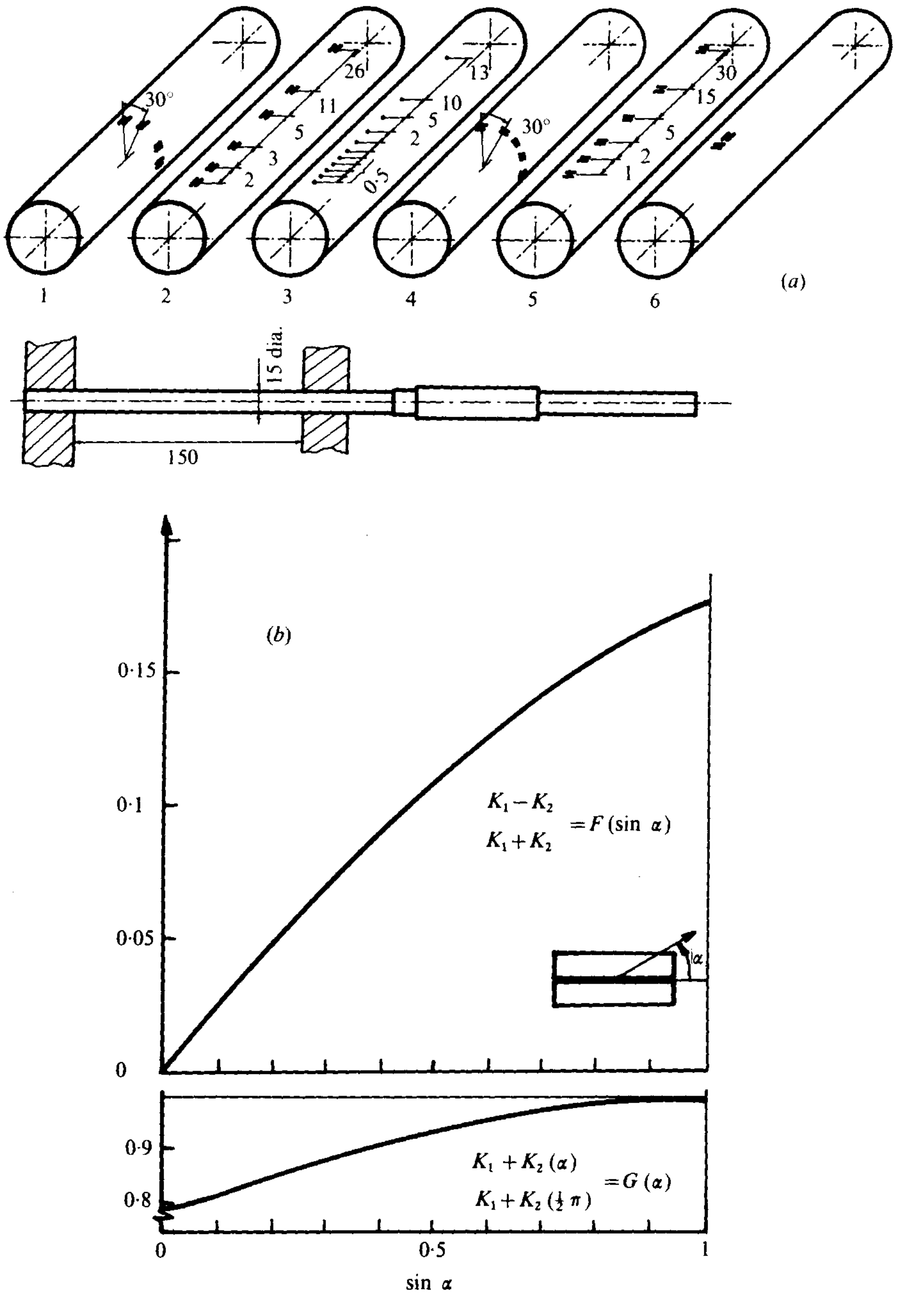

FIGURE 2. (*a*) Electrode array on the six cylinders. (Dimensions in mm.) (*b*) Calibration curve for electrode with aspect ratio 2·5.

ambiguities about the flow direction, which is then located in two quadrants; (iii) to allow significant measurements on the separation lines where the wall shear stress remains non-zero. The data processing consisted of separating out the time-averaged portion of the signal and distinguishing by auto- and cross-correlation and then by auto- and cross-spectral analysis the periodic portion from the random one.

The electrode array in figure 2 illustrates the way in which the spatial investigation was executed. Cylinder 6 is convenient for measuring the direction of the surface velocity gradient, the spectral analysis of every fluctuating component and also the local cross-spectral analysis between each velocity-gradient component. Cylinders 1 and 4 are convenient for cross-spectral analysis in the chordwise direction of the chordwise and spanwise components. Cylinders 2 and 5 are suited for cross-spectral analysis in the spanwise direction of the chordwise and spanwise components. Every spectrum and cross-spectrum available in this way for every azimuth cannot be given in the paper, but their main characteristics which allow the definition of six regions in which the flow-field structure is very different are described. The coherence of the periodic part of the fluctuations is determined. Its value enables a very precise significance to be attributed to the mean history of the integral wall streamlines, which will be constructed, instant by instant, from the measurements of the time-averaged magnitude and phase delay of the periodic fluctuations. In this degenerate case of three-dimensional fluctuating flow a direct verification of the independence principle and of the thermal analogy (Wild 1949) is made.

2. Interpretation of electrochemical measurements

Iodine reduction is used for convenience and better frequency response, but the electrochemical reaction

$$I_3^- + 2e \leftrightarrow 3I^-$$

is driven in such a manner (Reiss & Hanratty 1962) that the boundary conditions for the mass concentration field are not dependent on the flow:

$$C = 0 \quad \text{at the electrode,}$$

$$C = C_\infty \quad \text{in the far field,}$$

$$\partial C/\partial y = 0 \quad \text{at the insulated wall.}$$

The electrolysis current J_i on the part i of the area A_i of the electrode (figure 1, plate 1) provides a measurement of the space-averaged mass-transfer coefficient for the ionic active species. It can be expressed as

$$K_i = \frac{\mathscr{D}}{C_\infty}\frac{1}{A}\iint_{A_i}\left(\frac{\partial C}{\partial y}\right)_{y=0} dA = \frac{1}{C_\infty A}\frac{J_i}{2F}, \tag{1}$$

where F is Faraday's constant and $\mathscr{D}$ the diffusion coefficient. The transfer coefficient K_i is normalized by the entire area A of the split electrode so that it satisfies the same summation rule, $K = K_1 + K_2$, as the electrolysis current.

The first-order Taylor expansion of the velocity field about the centre of the transducer, taking into account the continuity equation and the no-slip condition, allows the velocity field to be characterized by two time-dependent parameters:

$$U_x = yS_{x0}(t), \quad U_y = 0, \quad U_z = yS_{z0}(t), \tag{2}$$

where $$S_{x0} = (\partial U_x/\partial y)_{x=y=z=0}, \quad S_{z0} = (\partial U_z/\partial y)_{x=y=z=0}.$$

As no hypothesis is made about the flow field, the transducer theory will be consistent for point electrodes if the numbers of the signals $K_i(t)$ and of the parameters $S_0(t)$ coincide.

The transfer equation (1) and the mass balance are normalized through the following transformation:

$$\left.\begin{aligned} &C^+ = C/C_\infty, \quad X^+ = X/l, \quad Z^+ = Z/l, \quad Y^+ = (Y/l)\,S_{x0}^{+\frac{1}{3}}, \\ &S^+ = Sl^2/\mathscr{D}, \quad t^+ = t\mathscr{D}S_{x0}^{\frac{2}{3}}/l^2, \quad n^+ = nl^2/\mathscr{D}S_{x0}^{\frac{2}{3}}, \quad K^+ = Kl/\mathscr{D}, \end{aligned}\right\} \tag{3}$$

l being a characteristic length of the electrode, n a frequency and t the time. Thus

$$K_i^+ = S_{x0}^{+\frac{1}{3}} \frac{1}{A} \iint_{A_i} \left(\frac{\partial C^+}{\partial y^+}\right)_{y^+=0} dA, \tag{4}$$

$$\frac{\partial C^+}{\partial t^+} = \frac{1}{S_{x0}^{+\frac{2}{3}}} \left[\frac{\partial^2 C^+}{\partial x^{+2}} + \frac{\partial^2 C^+}{\partial z^{+2}}\right] + \frac{\partial^2 C^+}{\partial y^{+2}} - y^+ \frac{\partial C^+}{\partial x^+} - \frac{S_{z0}}{S_{x0}} y^+ \frac{\partial C^+}{\partial z^+}. \tag{5}$$

In general the diffusion terms in the direction perpendicular to the wall dominate, as has been justified by numerous authors including Ling (1962). This is particularly true in liquids, where the diffusion coefficients are very small, so that S_{x0}^+ is important. The mass balance equation (5) simplifies to

$$\frac{\partial C^+}{\partial t^+} = \frac{\partial C^+}{\partial y^{+2}} - y^+ \frac{\partial C^+}{\partial x^+} - \frac{S_{z0}}{S_{x0}} y^+ \frac{\partial C^+}{\partial z^+}. \tag{6}$$

In a quasi-steady state, with the x axis in the flow direction, the mass balance (6) becomes a two-dimensional and universal equation. Then as a result of (4), each transfer coefficient K_i becomes proportional to $S_{x0}^{\frac{1}{3}}$ and the proportionality coefficient can be obtained by calibration. More generally, the quasi-steady-state solutions of (6) are dependent on only the electrode shape and the flow direction. Characteristic relationships for split-film electrochemical transducers may then be deduced very simply from (4) and (6). They can be written as a function of the angle α between the flow direction and the neutral axis of the transducer (figures 3*a*, *b*):

$$\frac{K_1^+ - K_2^+}{K_1^+ + K_2^+} = F(\alpha), \quad K_1^+ + K_2^+ = g\,G(\alpha)\,S_0^{+\frac{1}{3}}$$

with $$g = \text{constant}, \quad tg\alpha = S_{z0}/S_{x0}, \quad S_0 = (S_{x0}^2 + S_{z0}^2)^{\frac{1}{2}}. \tag{7}$$

K_1^+ and K_2^+ are the Sherwood numbers for each active area. Complete numerical solutions in three dimensions and measurements with split electrodes of various shapes and aspect ratios (Py 1973) show that these properties are not greatly modified by the diffusion terms in the wall direction. Any homogeneous combination of the transfer coefficient divided by another of the same degree depends only on the flow direction. Figure 2(*b*) shows the calibration curves $F(\alpha)$ and $G(\alpha)$ as a function of $\sin\alpha$ for rectangular electrodes with an aspect ratio of 2·5. From the two transfer signals K_1 and K_2 the surface velocity gradient and its direction are consistently deduced with a split point electrode. Let us note that single electrodes have already been used in three-dimensional flows. For example, Cognet (1971) calculated the mass transfer on single electrodes as a function of the flow pattern and detected the waves in a Couette flow. On a rotating disk, Chin & Litt (1972) used large aspect ratio electrodes and partially separated the fluctuating components of the velocity.

Small fluctuations: quasi-steady-state response

Let us choose the x component in the direction of the neutral axis (figure 3a) and separate each component into its time-averaged and fluctuating part:

$$C = \bar{C}+c, \quad K = \bar{K}+k, \quad S = \bar{S}+s.$$

If the fluctuations have a small amplitude, we can neglect the variations in $G(\alpha)$ and linearize (7). For $\alpha \neq \frac{1}{2}\pi$ one obtains

$$\frac{\overline{s_z^+}}{S_0^+} = \frac{1}{dF/d(\sin\alpha)}\frac{\overline{(k_1^+-k_2^+)}}{K_1^++K_2^+}+\left[3\sin\bar{\alpha}-\frac{F}{dF/d(\sin\bar{\alpha})}\right]\frac{\overline{(k_1^++k_2^+)}}{K_1^++K_2^+}, \tag{8}$$

$$\frac{\overline{s_x^+}}{S_0^+} = \frac{-tg\bar{\alpha}}{dF/d(\sin\alpha)}\frac{\overline{(k_1^+-k_2^+)}}{K_1^++K_2^+}+\left[3\cos\bar{\alpha}+tg\bar{\alpha}\frac{F}{dF/d(\sin\alpha)}\right]\frac{\overline{(k_1^++k_2^+)}}{K_1^++K_2^+}. \tag{9}$$

s_x and s_z are linear functions of k_1-k_2 and k_1+k_2. These fluctuations can be separated and determined in real time by executing the corresponding mixing of the signals. In practice, $\overline{s_x^2}$ and $\overline{s_z^2}$ are calculated from the measurements of $\overline{(k_1-k_2)^2}$, $\overline{(k_1+k_2)^2}$ and $\overline{(k_1-k_2)\,(k_1+k_2)}$. For $\alpha = 0$, (8) and (9) simplify to

$$\frac{\overline{s_z^+}}{S_0^+} = \frac{1}{dF/d(\sin\alpha)}\frac{\overline{k_1^+-k_2^+}}{K_1^++K_2^+}, \tag{10}$$

$$\frac{\overline{s_x^+}}{S_0^+} = 3\,\frac{\overline{k_1^++k_2^+}}{K_1^++K_2^+}. \tag{11}$$

If the angle α tends towards $\frac{1}{2}\pi$ (figure 3b), the transfer functions (7) can be written in the more suitable form

$$\left.\begin{aligned}(K_1^+-K_2^+)^3 &= g^3F^3(\tfrac{1}{2}\pi)\,[1-U(\alpha)]\,S_{z0},\\ (K_1^++K_2^+)^3 &= g^3[1-V(\alpha)]\,|S_{z0}|.\end{aligned}\right\} \tag{12}$$

Neglecting $U(\alpha)$ and $V(\alpha)$, which are generally small when α is high enough (Py & Tournier 1975a, b), equations (12) can be used directly with cubing electronic circuitry. For small fluctuations, linearizing (12) gives the results of Mitchell & Hanratty (1966):

$$\frac{\overline{k_1^+-k_2^+}}{K_1^+-K_2^+} = \frac{\overline{k_1^++k_2^+}}{K_1^++K_2^+} = \frac{1}{3}\frac{\overline{s_z}}{S_{z0}}. \tag{13}$$

Small fluctuations: frequency response

The inertia effect induced by the mass boundary layer on the transducer frequency response for small velocity fluctuations in the time-averaged flow direction has been calculated for single electrodes by Reiss & Hanratty (1963), Mitchell & Hanratty (1966) and Fortuna & Hanratty (1971). The frequency response for split electrodes has also been determined by Py (1973) for the configuration shown in figure 3(b). A linear combination of the collected signals on each half-electrode can considerably improve the transducer frequency response for these fluctuations. This result alone sometimes warrants the use of such a transducer.

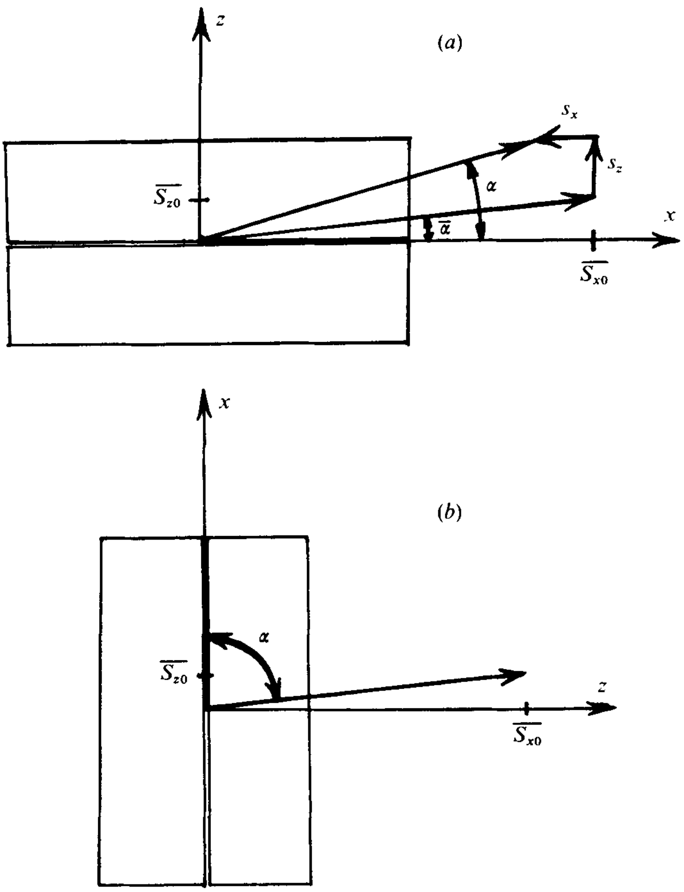

FIGURE 3. Electrode array. (*a*) First configuration. (*b*) Second configuration.

In the chevron array of Sirkar & Hanratty (1970), the fluctuations in the direction perpendicular to the time-averaged flow are detected from the opposite variation of the chordwise velocity component on each large aspect ratio electrode. The frequency response for these fluctuations can then be expressed in the same manner as that for chordwise fluctuations. But as this time-averaged component decreases with decreasing α, the response time is increased. In the case of the split electrodes in the configuration shown in figure 2, the frequency response is very different because the three-dimensional character of the concentration boundary layer must be taken into account. The calculation method consists of numerically simulating the evolution of the concentration field and the mass transfer in response to a spanwise step change (indicial response) in the surface velocity gradient. For small fluctuations the frequency response $f(n^+)$ is deduced from the indicial one and enables correction of the signal in Fourier space by the expression

$$k(n^+)/(\overline{k(t)^2})^{\frac{1}{2}} = f(n^+)\,s(n^+)/(\overline{s(t)^2})^{\frac{1}{2}}.$$

Figure 4 shows the amplitude and phase shift of an $f(n^+)$ function calculated in this way. Curves A and B relate to the frequency response for a small perturbation in the

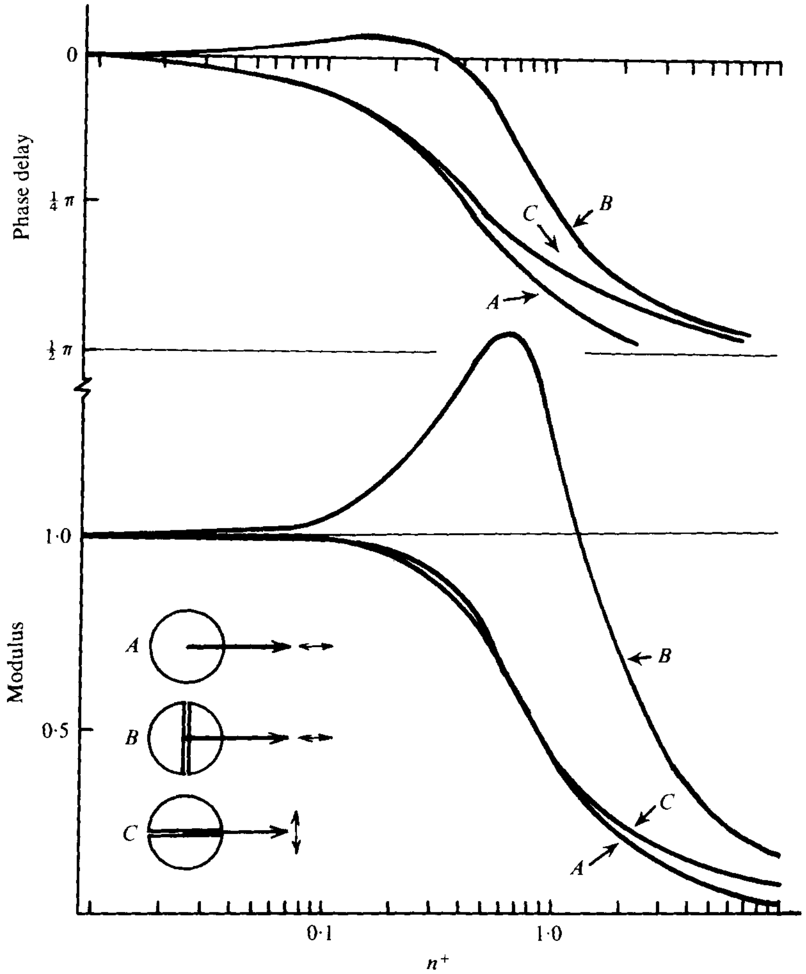

FIGURE 4. Frequency response of a split-film electrochemical transducer. A, single electrode, chordwise fluctuations; B, split electrode, chordwise fluctuations; C, split electrode, spanwise fluctuations.

flow direction for a single or a differential electrode respectively. As can be observed, the second sort of response is much more sensitive at high frequencies. In this particular case, the frequency response for small spanwise fluctuations (curve C) is closely similar to the response calculated in case A. For the cylinders used in this work, measurements need practically no corrections, whatever the azimuth is, as soon as the yaw angle reaches or exceeds 10°.

Spatial resolution

(i) With the previous set-up, from the two signals delivered by the split electrode we can determine only two unknowns, of which the most important are $S_{x0}(t)$ and $S_{z0}(t)$. Unfortunately, owing to the finite size of the transducer, if one can no longer consider $S(t)$ as independent of space, the method becomes inconsistent. Then the continuity equation implies the existence of a velocity component βy^2 perpendicular to the wall:

$$\partial S_x^+/\partial x^+ + \partial S_z^+/\partial z^+ + 2\beta^+ = 0.$$

Here we shall consider only an electrode in a cross-flow (figure 3*b*) or with a high enough aspect ratio that we can neglect the direct effect of spatial evolution of S_x.

Let us suppose $\partial S_z^+/\partial z^+ = 0$, which implies $\beta^+ = -\frac{1}{2}\partial S_x^+/\partial x^+$. Then the mass balance equation can be written in the form

$$\frac{\partial^2 C^+}{\partial y^{+2}} = y^+ \frac{\partial C^+}{\partial z^+} + (x^+ - x_0^+)\frac{\partial S_z^+}{\partial x^+}\frac{1}{S_{z0}^+} y^+ \frac{\partial C^+}{\partial z^+} + \frac{\beta^+}{S_{z0}^+} y^{+2} \frac{\partial C^+}{\partial y^+}.$$

For small β^+/S_{z0}^+, a first approximation of the general solution in terms of a Taylor expansion leads to

$$K_1^+ + K_2^+ = g S_{z0}^{+\frac{1}{3}}(1 - 0{\cdot}2\beta^+/S_{z0}^+), \tag{14}$$

$$K_1^+ - K_2^+ = g F(\tfrac{1}{2}\pi)\, S_{z0}^{+\frac{1}{3}}(1 + 0{\cdot}284\,\beta^+/S_{z0}^+). \tag{15}$$

S_{z0}^+ is obtained by combination of these equations as

$$S_{z0}^{+\frac{1}{3}} = g^{-1}[0{\cdot}589(K_1^+ + K_2^+) + 0{\cdot}413(K_1^+ - K_2^+)/F(\tfrac{1}{2}\pi)]. \tag{16}$$

Let us suppose now that $\partial S_x^+/\partial x^+ = 0$, which implies that to a first approximation

$$S_z = S_{z0} + (z - z_0)\frac{\partial S_z}{\partial z} + (x - x_0)\frac{\partial S_z}{\partial x}, \quad \beta l = -\frac{1}{2}\frac{\partial S_z}{\partial z}.$$

The Lévèque (1928) solution of the mass balance equation allows calculation of the first-order approximation of the transfer coefficient:

$$K_1^+ + K_2^+ = g S_{z0}^{+\frac{1}{3}}, \tag{17}$$

$$K_1^+ - K_2^+ = g F(\tfrac{1}{2}\pi)\, S_{z0}^{+\frac{1}{3}}\left[1 - \frac{2}{5}\frac{\partial S_z^+}{\partial z^+}\frac{1}{S_{z0}^+}\right]. \tag{18}$$

A systematic error is then introduced when $\partial S_x/\partial x$ or $\partial S_z/\partial z$ is neglected. However, relations (14), (15), (17) and (18) show that this error corresponds to a fundamental uncertainty in the measurement position smaller than half the width of an electrode. The fundamental uncertainty is consistently obtained by comparing the values of S_{z0} calculated from (16) and (17). This uncertainty proved to be quite small in the present work as a result of the compactness of the transducer.

(ii) Let us consider an electrode whose split axis is orientated in the flow direction (figure 3*a*) close to a separation line. To a first approximation, and for three-dimensional separation lines only, the velocity field is given by (Eichelbrenner 1957)

$$S_x = S_{x0}, \quad S_z = S_{z0} + (z - z_0)\,\partial S_z/\partial x,$$

with

$$S_{x0} \gg S_{z0}, \quad S_{x0} \gg \partial S_z/\partial x.$$

It has been shown (Tournier & Py 1973) that the new unknown $\partial S_z/\partial x$, which strongly modifies the response in the case of a two-dimensional separation, does not intervene in this case. The response of the split transducer obeys the characteristic equations (7). In the more general case of an electrode orientated in an arbitrary manner with respect to a three-dimensional separation line, S_{x0} and S_{z0} remain non-zero and relations (7) are always valid as the limiting law for sufficiently small electrodes.

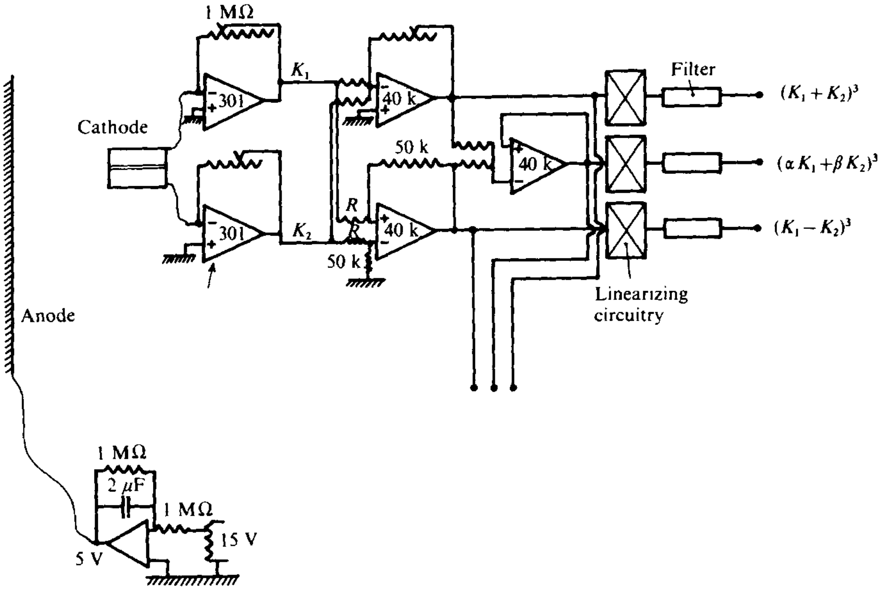

FIGURE 6. Schematic diagram of one circuit on the analog computer.

3. Experimental set-up

The hydraulic tunnel (figure 5, plate 2) is built from Altuglass 30 mm thick. A large platinum anode (150 × 80 mm) is embedded in the rear upper surface of the square 150 × 150 mm test section (1). One of the side walls is drilled to mount the cylinders, and fitted externally with a flexible silicone-based membrane, which allows the cylinders to be yawed without leaks. The large reservoir (2) upstream feeds the test section via a convergent nozzle with a 16 : 1 contraction ratio. The fluid is driven by an Altuglass propeller (3) which is attached to the shaft of a regulated motor (4). The heat exchanger (5) in the return section consists of parallel glass tubes. Temperature variations are less than 0·1 °C. Turning veins, honeycombs (6) and careful assembly resulted in low turbulence levels of the order of 0·6 % at a speed of 1 m/s. The support for the cylinders pivots on a vertical axis, allowing them to be yawed through angles up to 30° and to be rotated around their own axes.

The anode is kept at a constant potential of + 0·5 V. Each half-electrode is maintained at zero voltage by operational amplifiers operating in a common mode. Any required combination of the two signals is then obtained by a series of amplifiers and multiplexers on an analog computer. Four precision integrators enable us to make simultaneous measurements of time-averaged values and in particular to obtain very accurate correlation coefficients. Any point in the system could be connected to the appropriate measuring equipment through impedance adapters. For the different types of signal processing, a variety of special cables are used, but are not described here for brevity. Figure 6 illustrates the circuitry used to determine an autocorrelation function. As the frequencies are low (< 100 Hz) a real-time correlator manufactured by Intertechnique, consisting of a SA44 memory unit with 4000 channels and an L 10 correlation plug-in unit, gives the cross-correlation function of two signals. Other data treatment is executed on an IBM 1800 computer.

The six test cylinders (figure 2) are all 15 mm in diameter and completely span the test section. The electrochemical transducers are sealed with an acrylic resin. They are machined, carefully polished and degreased before use. The twin electrodes are made from two platinum ribbons, 0·5 × 0·1 mm in cross-section, separated by a strip of mylar 8 μm thick (figure 1, plate 1).

4. Results

Time-averaged components

Measured values of the time-averaged components of the surface velocity gradient are shown in figures 7 (*a*) and (*b*). Every related magnitude is dimensionless and normalized by the time-averaged chordwise component $(\overline{S_{x50}})$ for an azimuth of 50°. This value, which is very useful for the transducer calibration, has formed the subject of previous work (Achenbach 1968; Son & Hanratty 1969). In regions of low-level fluctuations, and particularly when the cylinder is yawed, every component is obtained from the time-averaged relations (7). When strong fluctuations changing direction occur, which is especially the case with the cylinder in cross-flow, we electronically linearize the signal difference from the electrode array on figure 3 (*b*), using expression (12).

In the upstream regions, measurements are in agreement with the predictions of boundary-layer theory (Sears 1948) except perhaps close to the upstream stagnation line, where the fluctuation rate increases indefinitely and Hiemenz's (1911) solution seems inadequate. In separated zones, just after the backflow region, the chordwise component remains quite small. Numerous authors, including Jones (1947), Görtler (1952), Nickel (1958) and Dienemann (1953), have shown that in laminar flows with 'cylindrical symmetry', i.e. when the boundary and volume forces are homogeneous in the generator direction, the chordwise velocity components are independent of the spanwise components. According to figure 7 (*a*), this independence principle (Jones 1947) seems well verified all around the cylinder for the time-averaged values, even in the separated zones, which indicates that the Reynolds stresses relative to the cross-flow are insensitive to yaw.

In addition, for a Prandtl number Pr of unity there is an analogy (Wild 1949; Sears 1948) between the spanwise flow on a yawed infinite cylinder and the temperature distribution in the same flow without dissipation with a uniform temperature at infinity and an isothermal wall. Figure 8 shows the variation of $NuRe^{-\frac{1}{2}}$, which represents the local heat transfer around a cylinder in a cross-flow (Schmidt & Wenner 1941; Martin 1969). The correction factor $Pr^{-\frac{1}{3}}$ is introduced to reduce the data to what they would effectively have been if the test had been carried out at $Pr = 1$. The same figure illustrates the evolution of the analogous group $Re^{-\frac{1}{2}}\partial(w/w_\infty)/\partial(y/D)$ corresponding to the spanwise velocity component w; these data fit well whatever the yaw is. It will be noticed that, for comparable Reynolds numbers, there is a good agreement between the very different experiments, even in separated zones.

Signal constitution

When the signals are electronically processed so as to separate (preserving its sign) the fluctuating part of any one velocity component, autocorrelation functions make the shedding frequency appear as a preferred one, the only one whose associated

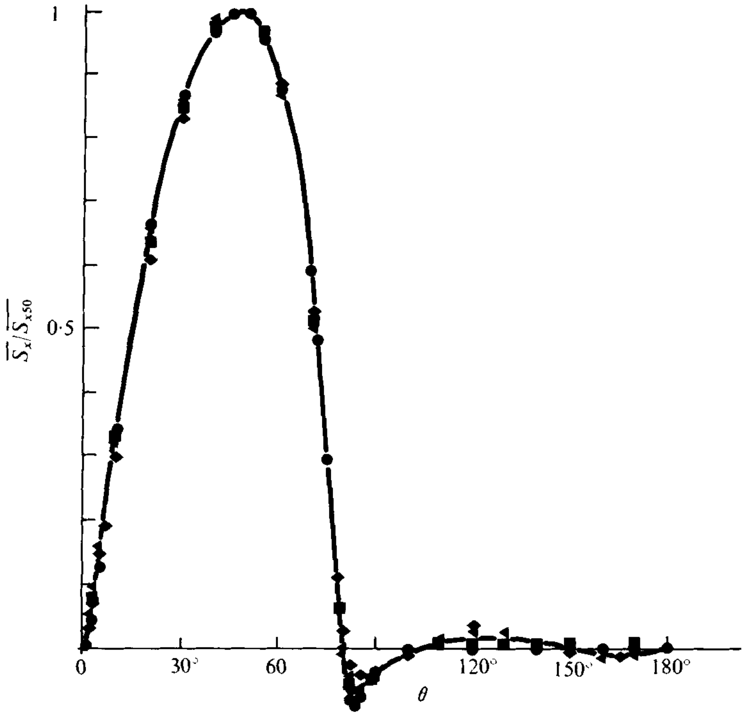

FIGURE 7 (*a*). For description see facing page.

power is significant. The signals are easily depicted in terms of the general formulae for clocks (Curtler & Searle 1966):

$$s(t) = u(t) + a_n[1 + f(t)] \cos [2\pi nt + \psi(t)], \tag{19}$$

where a_n represents the time-averaged amplitude of the periodic portion, $u(t)$ the random part of the signal, $f(t)$ a centred random function whose values are much smaller than unity for low Reynolds numbers and $\psi(t)$ a random function which characterizes the phase evolution. This last function is needed in order to explain why the correlation functions tend to zero and practically reach this value for a time delay which corresponds to about 100 periods. This periodic part is then a weakly deterministic one and its time evolution is satisfactorily interpreted as the result of phase fluctuations which follow a random-walk process. All information about the history of the flow field is forgotten after 100 periods, but during a short interval, 3 or 4 periods only, the damping of the correlation function for the periodic signal is negligible, so that its behaviour is deterministic. Figure 9 gives some examples of normalized auto-power spectra $\mathcal{S}_{uu}(0, 0, n)$ calculated from a Fourier transformation of the autocorrelation function. On account of the signal constitution, the peak for the shedding frequency cannot be classed as a Dirac distribution, i.e. the weight function which is used for the Fourier transformation enlarges it. However its area always corresponds to the power of the periodic signal. The ratios of this area to the area of the spectra of the chordwise and spanwise velocity components allow definition of the corresponding ratios γ_{uu} and γ_{ww} of the periodic portion.

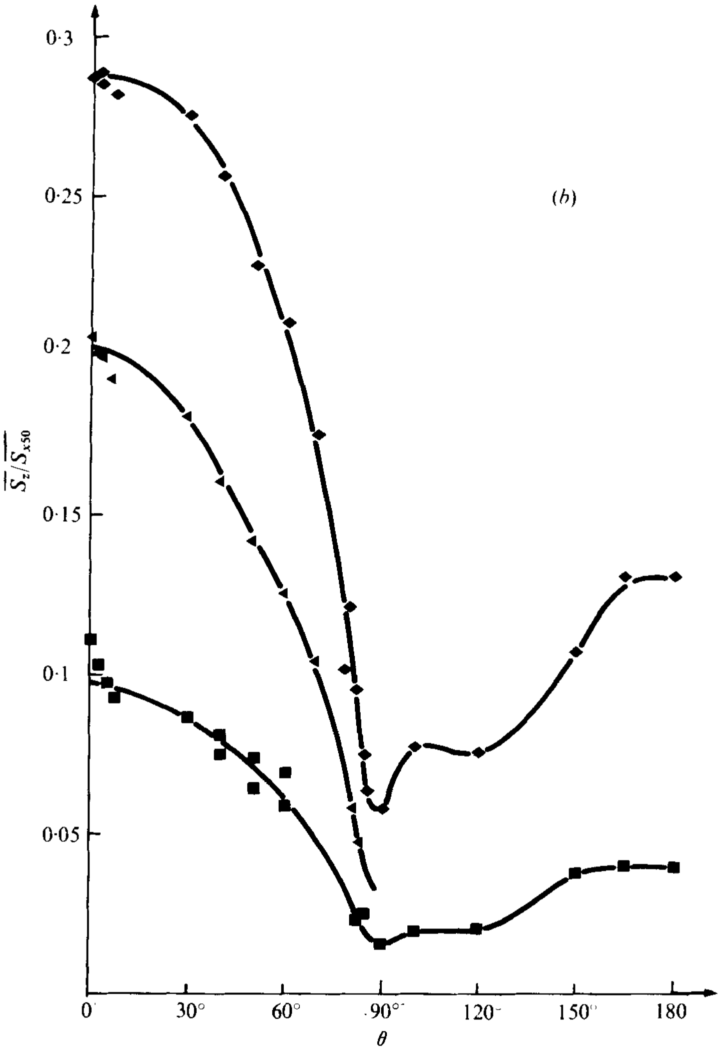

FIGURE 7. Azimuthal evolution of the time-averaged surface velocity. (*a*) Chordwise component. (*b*) Spanwise component. Yaw: ●, $\phi = 0$; ■, $\phi = 10°$; ◄, $\phi = 20°$; ◆, $\phi = 30°$.

These data are shown in figure 10, of which part (*a*) represents the evolution of γ_{uu} as a function of the azimuth. This periodic component is important in the boundary layer, in the backflow region and in the rear part of the separated zone. Very pronounced minima exist on the separation lines as though the static pressure forces, which obviously drive the movement directly on these lines, were more randomly distributed. In the intermediate zone ($\theta \simeq 110°$) the deterministic signal is quite small and completely hidden by random fluctuations. The evolution of the periodic spanwise component (figure 10*b*) has a very different character. It is negligible everywhere when the cylinder is in a cross-flow and, in every case, in the rearward region. It is significant only upstream of the separation line and increases with yaw.

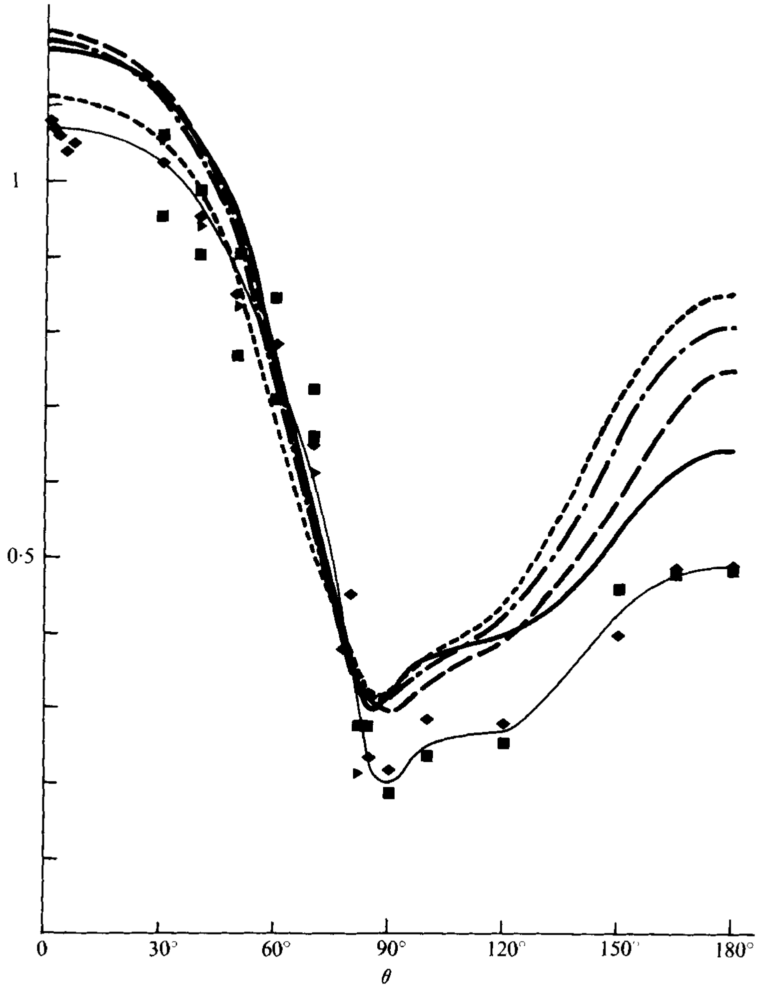

FIGURE 8. Thermal analogy. Wall gradient, $(\partial w/\partial y)\,(D/w_\infty)\,Re^{-\frac{1}{2}}$ ($Re = 13\,900$): ■, $\phi = 10°$; ◀, $\phi = 20°$; ◆, $\phi = 30°$. Heat transfer, $Nu/(Re^{\frac{1}{2}}Pr^{\frac{1}{3}})$: – – –, $Re = 52\,600$; —·—, $Re = 37\,400$; – –, $Re = 27\,500$; ——, $Re = 19\,500$.

Magnitude of fluctuations

Root-mean-square values of each component of the surface velocity gradient are shown on figure 11. The data were calculated from (8) and (10) or (12). For a yaw angle of zero and small time-averaged velocity, none of these equations can be applied for small aspect ratio electrodes, *a priori*. The results calculated according to (10) or (12), for the corresponding arrangement of the transducers, are drawn as dashed lines. They differ from each other but those which were calculated from (10) are in good agreement with the other results obtained when the cylinder was yawed. This supports the fact that the entire mass transfer on a single electrode depends in this case on the absolute velocity gradient and cannot be ascribed to a pure diffusion effect, which would be much smaller.

Rather than discuss the results for the root-mean square value of each fluctuating component, it seems more significant to distinguish which correspond to the periodic

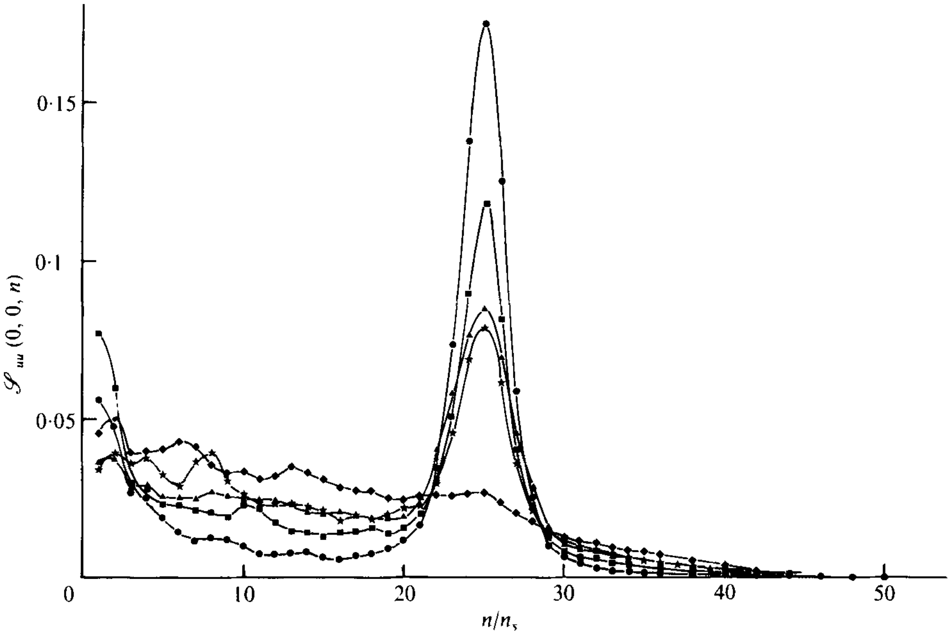

FIGURE 9. Power spectra for the chordwise velocity component. Yaw = 15°. ●, $\theta = 10°$; ■, $\theta = 60°$; ▲, $\theta = 90°$; ◆, $\theta = 120°$; ★, $\theta = 180°$.

fluctuations $[(\gamma_{uu}\overline{s_x^2})^{\frac{1}{2}}$ and $(\gamma_{ww}\overline{s_z^2})^{\frac{1}{2}}]$ and which correspond to the random fluctuations $[\{(1-\gamma_{uu})\overline{s_x^2}\}^{\frac{1}{2}}$ and $\{(1-\gamma_{ww})\overline{s_z^2}\}^{\frac{1}{2}}]$ since their azimuthal evolutions are very different. Periodic fluctuations of the chordwise component are of essential importance and their azimuthal evolution is similar to that of the ratio of their periodic powers (figure 10*a*). Their level is appreciable in the entire boundary layer with two minima on the upstream stagnation line and close to the separation line, respectively. In separated zones, periodic fluctuations are very important in the backflow region ($80° < \theta < 90°$) and in the region at the rear of the cylinder ($150° < \theta < 180°$) but they vanish in the intermediate region. As far as the random fluctuations are concerned, the chordwise component is at once dominant in the boundary layer. After separation, this component quickly decreases as in figure 11, whereas the magnitude of the spanwise fluctuations increases monotonically. The ratio reaches 10 for an azimuth of 100°. Then the flow mainly oscillates in the spanwise direction as has been shown only by visualization techniques (Son & Hanratty 1969). At higher azimuths, the magnitudes of all the components tend to reach a similar level.

Cross-spectra and phase evolution

Cross-power spectra between the values of any velocity component at two points are obtained by Fourier transformation of cross-correlation functions. They allow the measurement of the complex ratios $\gamma_{uw}(\theta, z, n_s)$ by division of the area of the real and imaginary peaks by the area of the real spectra. Phase delays could be calculated by comparing the real and imaginary parts of $\gamma_{uw}(\theta, z, n_s)$. In practice, for an azimuth difference exceeding 30°, the random part of signals does not appear in these spectra and the cross-correlation function looks like a slowly damped sine curve. Then the

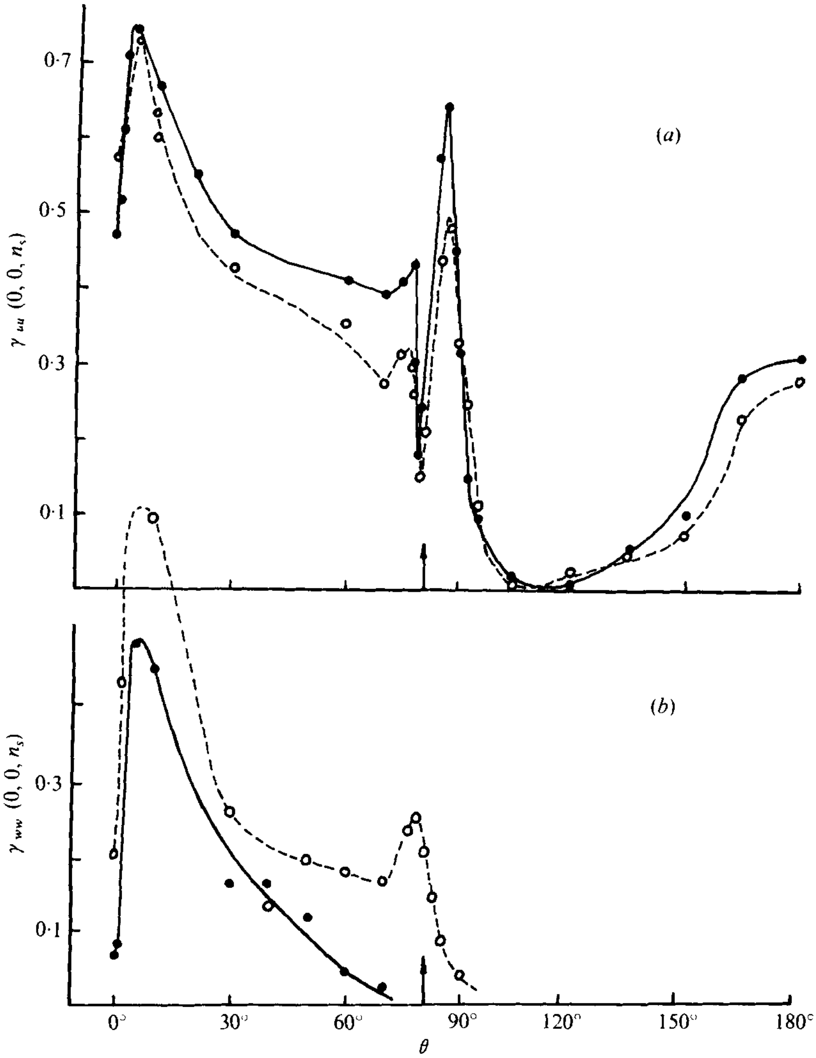

FIGURE 10. Azimuthal evolution of the periodic part of the signal power. (*a*) Chordwise component: ——, yaw = 0; – – –, yaw = 15°. (*b*) Spanwise component: ——, yaw = 10°; – – –, yaw = 30°.

phase delay corresponds to the phase displacement at the origin of the cross-correlation function.

Figure 12 (*a*) shows the evolution of the time-averaged phase delay $\overline{\Delta\phi}$ of the chordwise component of the surface velocity gradient. The phase origin is chosen as $\theta = 0$ although the reference transducer is always located close to $\theta = 180°$, where this delay does not evolve. As the curvilinear chordwise axis at the wall is chosen to be periodic in space, phase delays are the same on the upper and lower sides of the cylinders. Upstream stagnation and separation lines are characterized by a very sharp phase advance. This effect is partly explained by the fact that viscosity and inertia forces are small and pressure forces act instantaneously in these regions, on the flow direction. As a consequence, vorticity exists on these lines.

Figure 12 (*b*) represents the phase evolution of the spanwise component with

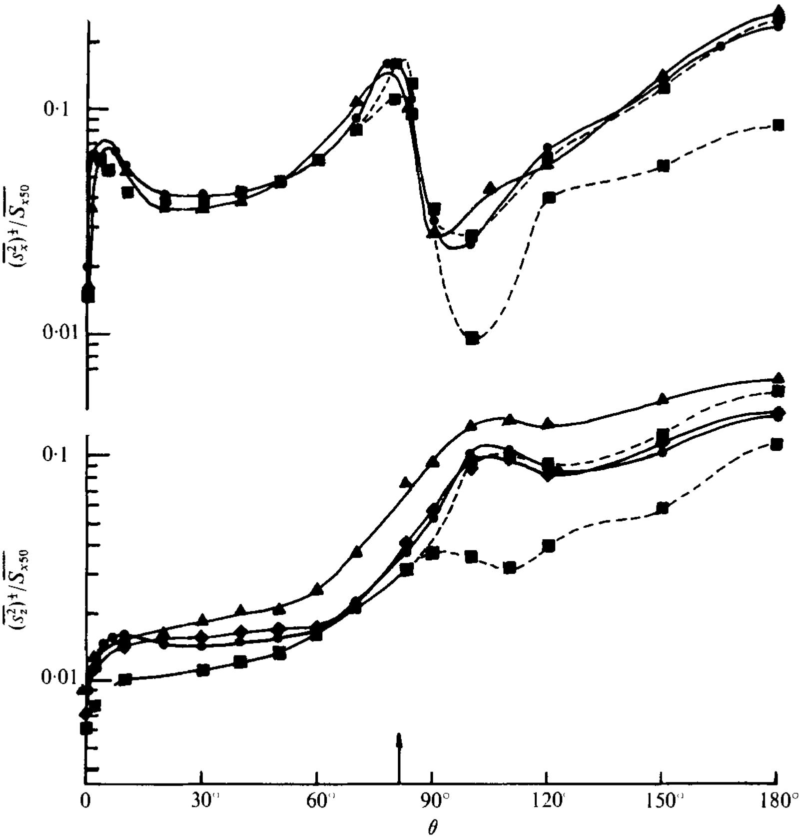

FIGURE 11. Azimuthal evolution of the root-mean-square values for chordwise and spanwise fluctuations. Yaw: ■, 0; ●, 10°; ◆, 20°; ▲, 30°.

regard to the same origin. The hypothesis that the probability of observing a sequence in the flow pattern is equal to the probability of observing the symmetrical sequence requires that generally (Py & Tournier 1975*a*, *b*) the transverse velocity fluctuations are of opposite phase at two symmetrical points on the cylinder. Thus statistically,

$$\langle s_z(\theta,t)|\phi_{\mathrm{ref}}\rangle = -\langle s_z(-\theta,t)|\phi_{\mathrm{ref}}\rangle,$$

and in the limit $\theta \rightarrow 0$, $\langle s_z(\theta,t)|\phi_{\mathrm{ref}}\rangle$ should tend statistically to zero. Figure 10(*b*) clearly illustrates the drop in the periodic part of this component on the upstream stagnation line, and figure 12(*b*) the 180° phase change which ensures the spatial antisymmetry of the periodic flow around the yawed cylinder.

Figure 13 gives an example of cross-power spectra $\mathscr{S}_{uu}(0,z,n)$ at two points on the same generator; similar spectra have been observed whatever the azimuth, the yaw angle or the velocity component. The cross-power peak is real and the time-averaged phase delay does not exist. On this point periodic movement well satisfies the independence principle. However the imaginary parts of the spectrum show that a convection velocity in the generator direction exists when the cylinder is yawed, for random perturbations.

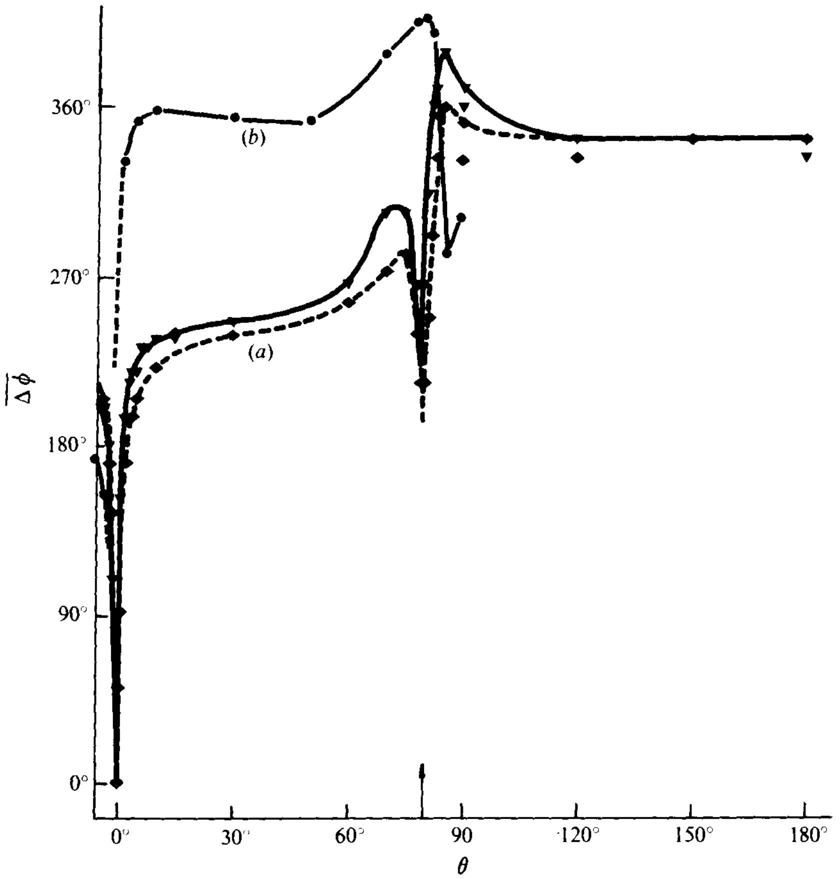

FIGURE 12. Azimuthal evolution of the time-averaged phase delay. (a) Chordwise component. (b) Spanwise component. Yaw: ▼, 0; ●, 10°; ◆, 15°.

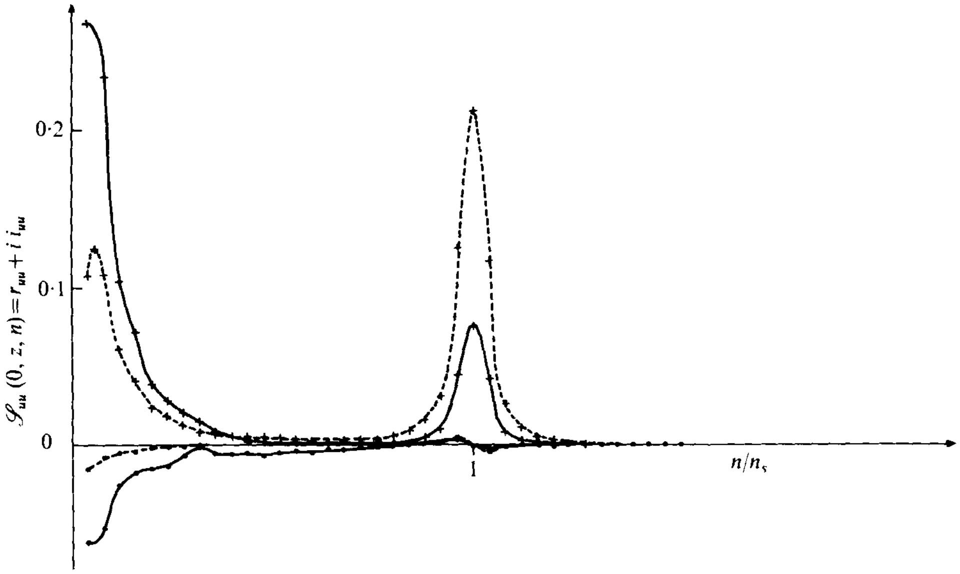

FIGURE 13. Cross-power spectra between two points on the same generator. – –+– –, r_{uu}, $\theta = 0$; – –●– –, i_{uu}, $\theta = 0$; —+—, r_{uu}, $\theta = 80°$; —●—, i_{uu}, $\theta = 80°$.

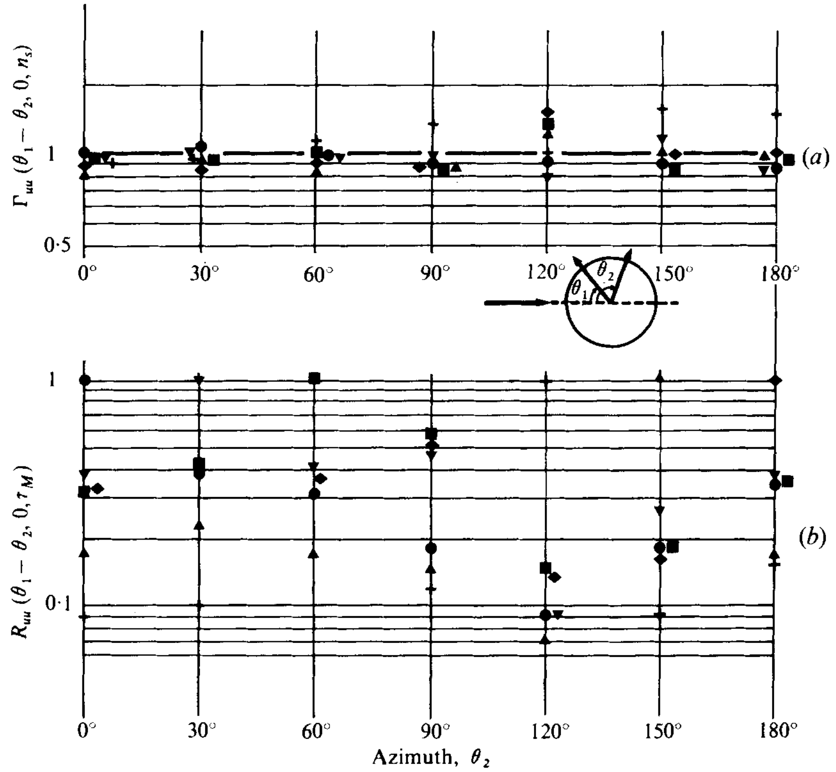

FIGURE 14. Double azimuthal evolution of (*a*) the coherence of the periodic part of S_x and (*b*) the maximum absolute value of the correlation functions. ●, $\theta_1 = 0$; ▼, $\theta_1 = 30°$; ■, $\theta_1 = 60°$; +, $\theta_1 = 120°$; ▲, $\theta_1 = 150°$; ◆, $\theta_1 = 180°$.

Coherence

The ratios of the periodic powers and the cross-power γ_{uu}, γ_{ww} and γ_{uw} (θ, z, n) and the correlation coefficient R_{uw} $(\theta, z, 0)$ allow calculation of the coherence of the periodic portion

$$\Gamma_{uw}(\theta, z, n_s) = \frac{\left|\int_{n_s-\Delta n}^{n_s+\Delta n} \mathscr{S}_{uw}(\theta, z, n)\, dn\right|}{\left(\int_{n_s-\Delta n}^{n_s+\Delta n} \mathscr{S}_{uu}(n)\, dn \int_{n_s-\Delta n}^{n_s+\Delta n} \mathscr{S}_{ww}(n)\, dn\right)^{\frac{1}{2}}} \tag{20}$$

from the formula
$$\Gamma_{uw}(\theta, z, n_s) = \frac{|\gamma_{uw}(\theta, z, n_s)|}{(\gamma_{uu}\ \gamma_{ww})^{\frac{1}{2}}} R_{uw}(\theta, z, 0). \tag{21}$$

In practice, the results can have high errors if the periodic-power ratios γ_{uu} or γ_{ww} are small. The lower part of figure 14 illustrates the maximum of the cross-correlation function of the chordwise velocity component between two points on the same circular cross-section. This maximum considerably changes depending upon the positions θ_1 and θ_2 of the two points. But in the upper part of the same figure, we observe that the coherence $\Gamma_{uu}(\theta_2-\theta_1, 0, n_s)$ for the shedding frequency n_s remains remarkably close to unity for all θ_1 and θ_2. The scatter in some of the data at θ_1 or $\theta_2 = 120°$ is due to measurement errors in this region, where the periodic motion has

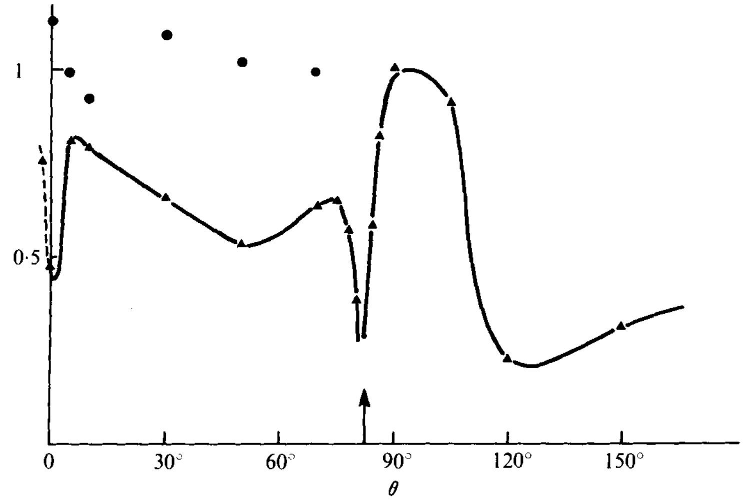

FIGURE 15. Azimuthal evolution of the local coherence (circles) and the maximum value of the correlation function (triangles) between every velocity component.

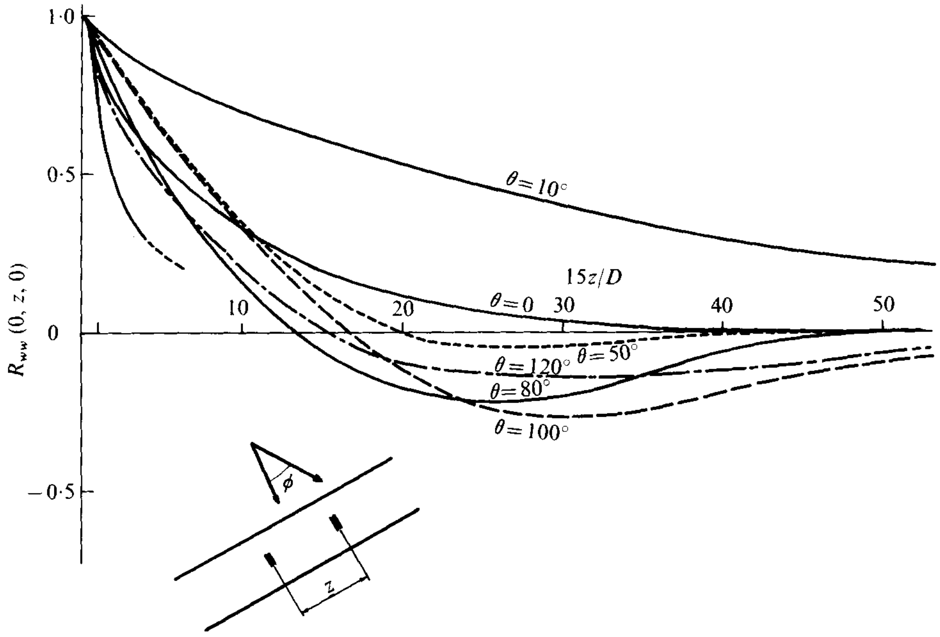

FIGURE 16. Spanwise evolution of the correlation coefficient for the spanwise velocity component.

little effect. The good agreement of the other results indicates that the overall periodic motion is coherent.

The local coherence $\Gamma_{uw}(0, 0, n_8)$ between each component is shown on figure 15 for azimuths where this quantity is significant. We observe that it is also close to unity. As a result of the general properties of coherence functions (Renyi 1966) periodic spanwise fluctuations are also coherent upon any cross-section and the coherence functions $\Gamma_{uu}(0, z, n_s)$ and $\Gamma_{ww}(0, z, n_s)$ in the spanwise direction are not dependent on the azimuth. This inference has been found to be well satisfied. In fact, the coherence remains close to unity in the spanwise direction for a distance of two diameters, but its integral scale is of the order of the channel width and cannot be measured.

Another important result can be observed on figure 15. In a region where periodic fluctuations are not significant ($90° < \theta < 110°$), the maximum value of the local correlation coefficient between each component is unity. They are then connected by a linear relation and coherent for any frequency. Also, for the same azimuth the correlation coefficient $R_{uw}(0, z, 0)$ (figure 16) approaches zero only when the distance between the transducers exceeds 4 diameters. These distances are large when compared with the other length scales of random movements. As an exchange of power or information between the periodic movements at the different cross-sections of the cylinder is needed in order to explain why the flow oscillates in step over large distances, it is probably in this region, owing to this random spanwise velocity component, that the exchange appears. Downstream, for $\theta \simeq 180°$, random fluctuations are less coherent and much more characteristic of turbulence.

Reconstitution of the flow pattern

On choosing a reference phase at some point, the time evolution of the surface velocity gradient can be written for any other point as

$$s(t) = u(t) + a_n \cos[\phi_{\text{ref}} + \Delta\phi(t)], \tag{22}$$

with

$$\phi_{\text{ref}} = 2\pi n_s t + \psi(t).$$

Separating the random part of the phase delay between the reference point and the selected point, from the time-averaged delay we have

$$\Delta\phi(t) = \overline{\Delta\phi} + \Delta\varphi(t).$$

The conditional phase average can be written as

$$\langle s(t) | \phi_{\text{ref}} \rangle = a_n \overline{\cos[\Delta\varphi(t)]} \cos[\phi_{\text{ref}} + \overline{\Delta\phi}]. \tag{23}$$

From the coherence definition (20) it can be shown easily that $\overline{\cos[\Delta\varphi(t)]} = 1$ when the periodic flow is coherent. Then not only will the reconstitution of this periodic part from its time-averaged magnitude and phase delay have the same significance as a phase conditional average, but also the flow configuration will be independent of the selected reference point.

Rather than doing a direct reconstitution, the conditional phase-averaged values are decomposed in the form of a double Fourier series taking into account the periodic character of the flow in space and time:

$$\frac{\langle s_x(\theta, t) | \phi \rangle}{S_{x50}} = \sum_{m=-\infty}^{+\infty} \left(\frac{A_m}{\pi} \cos\phi - \frac{A'_m}{\pi} \sin\phi \right) \cos m\theta, \tag{24}$$

$$\frac{\langle s_z(\theta, t) | \phi \rangle}{S_{x50}} = \sum_{m=-\infty}^{+\infty} \left(\frac{B_m}{\pi} \cos\phi - \frac{B'_m}{\pi} \sin\phi \right) \sin m\theta, \tag{25}$$

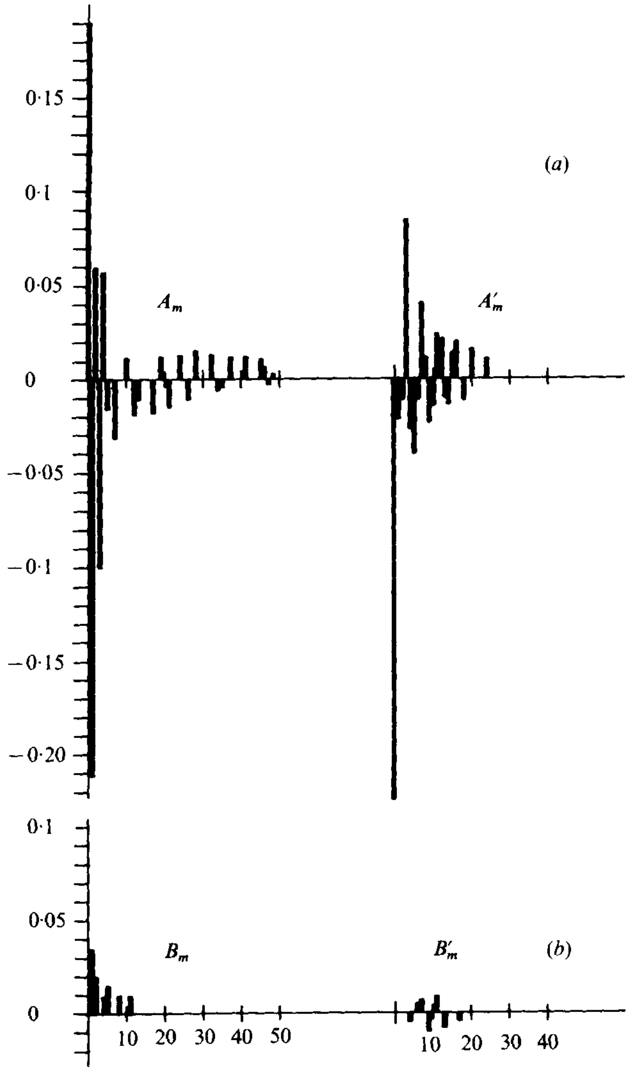

FIGURE 17. Wavenumber spectra of the periodic fluctuations around a cross-section. (a) Chordwise component. (b) Spanwise component.

with

$$A_m = \int_0^\pi \left(2\gamma_{uu}\frac{\overline{(s_x)^2}}{S_{x50}}\right)^{\frac{1}{2}} \cos\overline{(\Delta\phi)}\cos(m\theta)\,d\theta,$$

$$A'_m = \int_0^\pi \left(2\gamma_{uu}\frac{\overline{(s_x)^2}}{S_{x50}}\right)^{\frac{1}{2}} \sin\overline{(\Delta\phi)}\cos(m\theta)\,d\theta,$$

$$B_m = \int_0^\pi \left(2\gamma_{ww}\frac{\overline{(s_z)^2}}{S_{x50}}\right)^{\frac{1}{2}} \cos\overline{(\Delta\phi)}\sin(m\theta)\,d\theta,$$

$$B'_m = \int_0^\pi \left(2\gamma_{ww}\frac{\overline{(s_z)^2}}{S_{x50}}\right)^{\frac{1}{2}} \sin\overline{(\Delta\phi)}\sin(m\theta)\,d\theta.$$

Negative values of m are introduced to simplify the equations. Symmetry conditions require

$$A_m = A_{-m}, \quad A'_m = A'_{-m}, \quad B_m = -B_{-m}, \quad B'_m = -B'_{-m}.$$

Figure 17 shows the complex magnitude of the coefficients associated with each chordwise wavenumber for the two components. The 'zero wave', which corresponds to the global oscillating fluid movement around the cylinder surface and tends to swivel the cylinder, and the first wave are the most important ones. But although these results are interesting in showing the phase array between each wave and allow reduction to a minimum of the number of coefficients needed for the description of the flow, no simple interpretation can be given. The wavenumber structure is highly complicated and in order to represent the flow correctly it is necessary to take into account a sufficiently large number of lines ($m \geqslant 41$).

In addition to the time-averaged values of each component of the wall velocity gradient, the corresponding phase conditional averages (24) and (25) give the instantaneous deterministic configuration of the surface flow. Figure 18 shows, in polar co-ordinates, the evolution of the chordwise component during half a period divided into 24 parts. In order to avoid discontinuities for $\theta = 0$ and $\theta = 180°$, S_x is taken as positive when it is directed in the same sense as the arrow. The flow configuration is shown as dashed lines and the separation points occur when the $\langle S_x(t)|\phi_{\text{ref}}\rangle$ curve intersects the circle of zero wall shear stress. The shedding of a rear vortex occurs at times $8/24n_s$ and $20/24n_s$, when a new contrary vortex forms at the wall on the rear side.

Integral wall streamlines are represented during one period for a yaw angle of 10° on figure 19. From the measurements, it cannot be determined whether the separation lines are envelopes or asymptotes of integral lines. In the region extending from 90° up to 110°, where the information exchange keeping the flow pattern homogeneous in the spanwise direction arises, integral lines are mainly directed in this direction at any time. The rearward separation line is quickly displaced from this region to the symmetrical one. At these instants, a small phase advance in the spanwise direction must induce a very complicated three-dimensional configuration for the rearward separation line. If, for example, the downstream cross-section is at point 20 in the cycle while the upstream section is at point 18, the backflow zone (in the downstream cross-section) is well separated from the rear zone of its own section, but it is connected to the rear zone of the upstream cross-section. Then phase information can easily be exchanged over large distances in the generator direction. Other interesting structures occur on the stagnation or separation lines. Figures 20 (*a*) and (*b*) illustrate respectively the streamlines in the latter regions at different points in the cycle. In the neighbourhood of the upstream stagnation point, starting from the initial configuration, the low speed zone enlarges until two counter-rotating vortices form which quickly displace the stagnation point. At the half-period, one returns to a configuration symmetric with repect to the first and the pattern then continues in a symmetric fashion. In the case of the separation line, the mechanism is no longer symmetric. The backward displacement of the separation line occurs very suddenly whilst the forward return is more gradual. The previous representations are purely qualitative since only the wall gradient is known and the random movement is always present and makes the instantaneous flow configuration strongly different from the conditional phase-averaged flow. Although the extrapolations from the wall must be treated

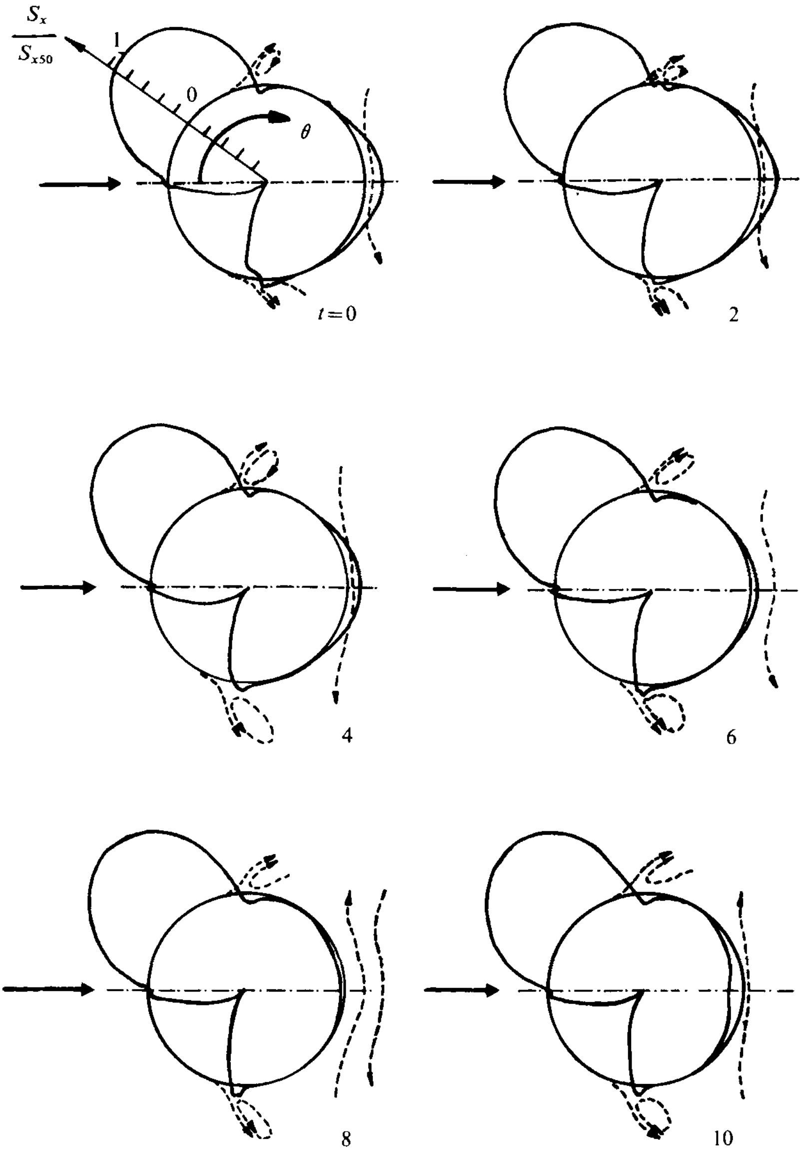

FIGURE 18. Reconstitution of the conditionally averaged chordwise wall gradient around a cross-section during a half-period divided into 12 parts.

carefully they do seem to give a plausible picture. In any case the evolution of the wall gradient shows the existence of some fairly complicated coherent structures. In particular, at certain times, the stagnation and separation zones possess multiple points of zero skin friction. This unusual phenomenon is similar to the 'double zero shear stress phenomenon' found by Dwyer & McCroskey (1973) in the separation region, from a boundary-layer calculation based on external flow measurements. Although Dwyer & McCroskey do not give a detailed description of their results, it would seem that the phenomenon is the same. The relationship between the movement of the instantaneous stagnation and separation points is difficult to obtain,

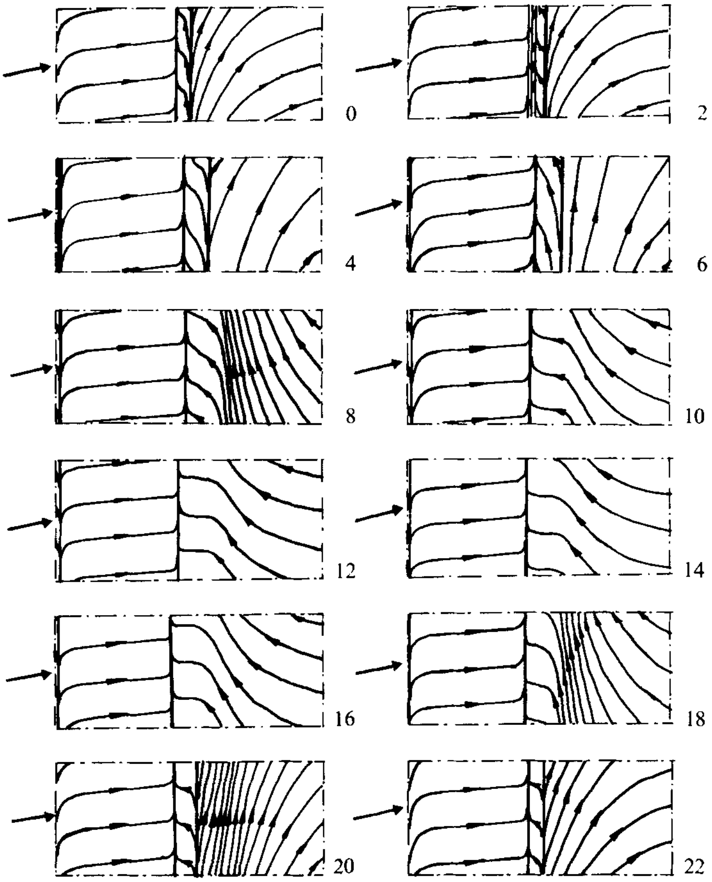

Figure 19. Reconstitution of the conditionally averaged integral wall streamlines during one period divided into 24 parts.

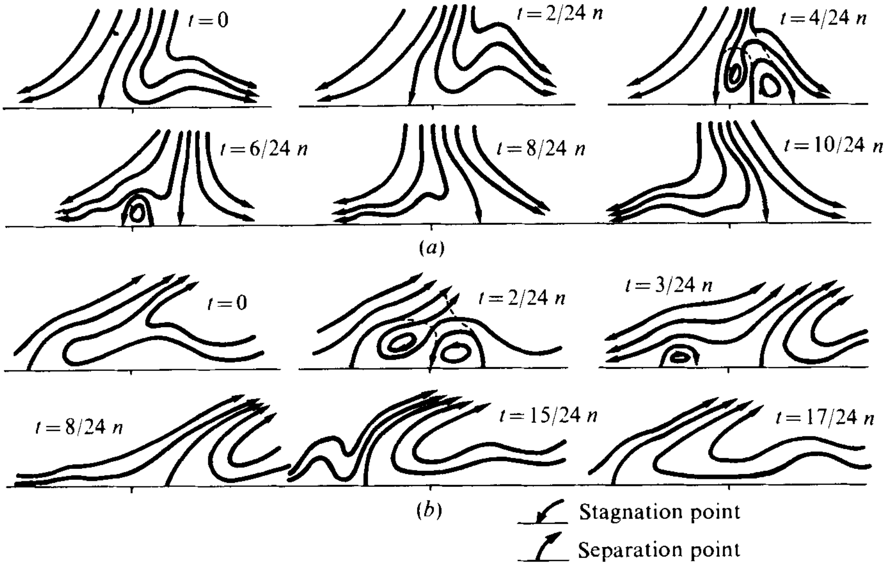

Figure 20. (*a*) Mean streamlines for zero azimuth. (*b*) Mean streamlines for separation azimuth.

since the complexity of the flow in the stagnation zone is much greater than they supposed. Their results imply that, in order to account for such chordwise velocity variations, the signal must be subjected to a very rapid spatial phase change and this is well observed. An analogous situation exists at the upstream separation point, and any theoretical study must take this into account.

REFERENCES

Achenbach, E. 1968 *J. Fluid Mech.* **34**, 625–639.

Batham, J. P. 1973 *J. Fluid Mech.* **57**, 209–228.

Bellhouse, B. J. & Schultz, D. L. 1966 *J. Fluid Mech.* **24**, 379–400.

Chin, D. T. & Litt, M. 1972 *J. Fluid Mech.* **54**, 613–625.

Cognet, G. 1971 *J. Méc.* **10**, 65–89.

Curtler, L. S. & Searle, C. L. 1966 *Proc. I.E.E.E.* **54**, 136–154.

Dienemann, W. 1953 *Z. angew. Math. Mech.* **33**, 89–109.

Dimopoulos, H. D. & Hanratty, T. J. 1968 *J. Fluid Mech.* **33**, 303–319.

Dwyer, H. A. & McCroskey, W. J. 1973 *J. Fluid Mech.* **61**, 753–767.

Eichelbrenner, E. A. 1957 *ONERA Publ.* no. 89.

Fortuna, G. & Hanratty, T. J. 1971 *Int. J. Heat Mass Transfer* **14**, 1499–1507.

Görtler, H. 1952 *Arch. Math.* **3**, 216–231.

Hiemenz, K. 1911 *Dingl. Polytech. J.* **326**, 321–342.

Jones, R. T. 1947 *N.A.C.A. Tech. Note* no. 1402.

Karabelas, A. J. & Hanratty, T. J. 1968 *J. Fluid Mech.* **34**, 159–162.

Lévêque, M. A. 1928 *Ann. Mines* **13**, 201–243.

Ling, S. C. 1962 *J. Heat Transfer* C **85**, 230–234.

Loiseau, H. & Szechenyi, E. 1972 *Rech. Aérosp.* **5**, 279–291.

McCroskey, W. J. & Durbin, E. J. 1972 *A.S.M.E. J. Basic Engng.* D **94**, 46–52.

Martin, M. 1969 Thèse, Université de Nancy.

Mitchell, J. E. & Hanratty, T. J. 1966 *J. Fluid Mech.* **26**, 199–221.

Nickel, K. 1958 *Arch. Math.* **9**, 313–320.

Py, B. 1973 *Int. J. Heat Mass Transfer* **16**, 129–144.

Py, B. & Tournier, C. 1975*a* *DRME Rep.* no. 73–805.

Py, B. & Tournier, C. 1975*b* *Proc. 4th Biennial Symp. Turbulence in Liquids, Univ. Missouri, Rolla*, pp. 266–276.

Reiss, L. P. & Hanratty, T. J. 1963 *A.I.Ch.E. J.* **9**, 154–160.

Renyi, A. 1966 *Calcul des Probabilités.* Paris: Dunod.

Schmidt, E. & Wenner, K. 1941 *Forschung.* **12**, 65–73.

Sears, W. R. 1948 *J. Aero. Sci.* **15**, 49–52.

Sirkar, K. K. & Hanratty, T. J. 1970 *J. Fluid Mech.* **44**, 605–614.

Son, J. S. & Hanratty, T. J. 1969 *J. Fluid Mech.* **35**, 353–368.

Surry, D. 1972 *J. Fluid Mech.* **52**, 543–563.

Tournier, C. & Py, B. 1973 *C. R. Acad. Sci. Paris* **277**, 1187–1190.

Werlé, H. 1959 *Rech. Aérosp.* **70**, 15–23.

Werlé, H. 1960 *Rech. Aérosp.* **79**, 9–26.

Werlé, H. 1962 *Rech. Aérosp.* **90**, 14–20.

Wild, J. M. 1949 *J. Aero. Sci.* **16**, 41–45.

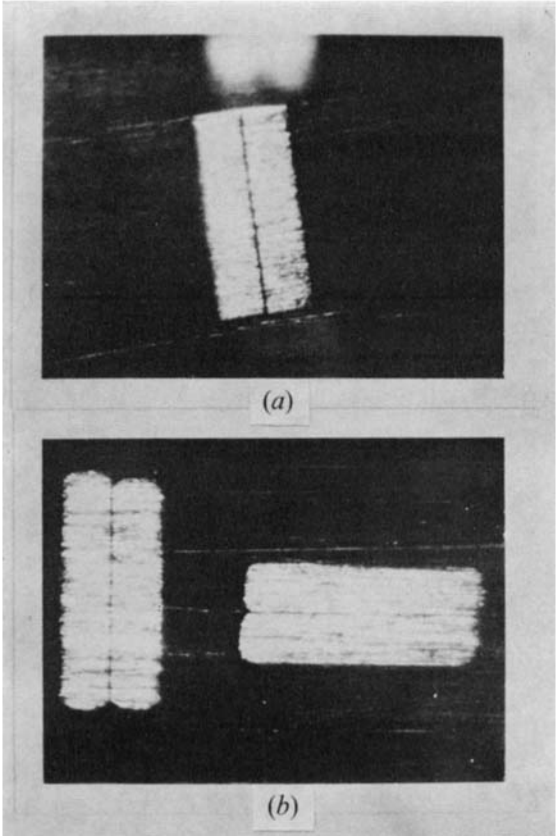

FIGURE 1. Split electrodes. (*a*) Cylinder 5. (*b*) Cylinder 6.

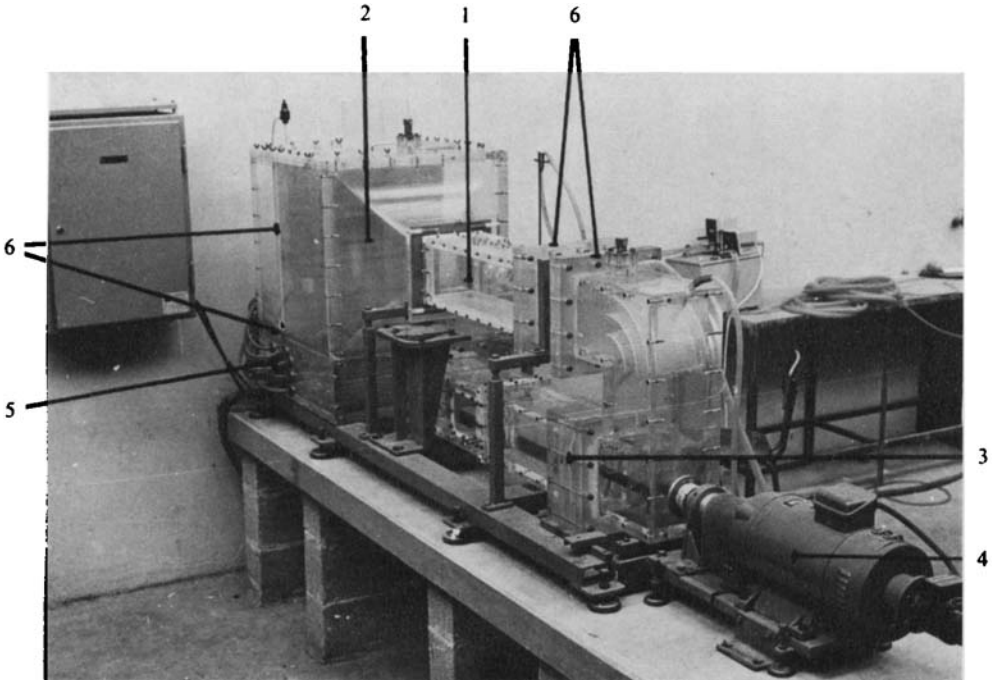

FIGURE 5. Hydraulic channel.